remote sensing

MDPI

Article

Cross-Validation of GEMS Total Ozone from Ozone Profile and Total Column Products Using Pandora and Satellite Observations

Sungjae Hong [1], Juseon Bak [2,*], Arno Keppens [3], Kai Yang [4], Kanghyun Baek [5], Xiong Liu [6], Mijeong Kim [7], Jhoon Kim [8], Lim-Seok Chang [7], Hyunjin Lee [1] and Jae-Hwan Kim [1]

[1] Department of Atmospheric Sciences, Pusan National University, Busan 46241, Republic of Korea; sungjae@pusan.ac.kr (S.H.); iamhyunjin@gmail.com (H.L.); jaekim@pusan.ac.kr (J.-H.K.)
[2] Institute of Environmental Studies, Pusan National University, Busan 46241, Republic of Korea
[3] Royal Belgian Institute for Space Aeronomy (BIRA-IASB), 1180 Brussels, Belgium; arno.keppens@aeronomie.be
[4] Department of Atmospheric and Oceanic Science, University of Maryland, College Park, MD 20742, USA; kaiyang@umd.edu
[5] NASA Goddard Space Flight Center, Greenbelt, MD 20771, USA; kanghyun.baek@nasa.gov
[6] Atomic and Molecular Physics Division, Center for Astrophysics | Harvard & Smithsonian, Cambridge, MA 02138, USA; xliu@cfa.harvard.edu
[7] National Institute of Environmental Research, Incheon 22689, Republic of Korea; mjkim48@korea.kr (M.K.); lschang@korea.kr (L.-S.C.)
[8] Department of Atmospheric Sciences, Yonsei University, Seoul 03722, Republic of Korea; jkim2@yonsei.ac.kr
* Correspondence: juseonbak@pusan.ac.kr

Highlights

What are the main findings?

- The reprocessed GEMS v3.0 ozone profile (O_3P) product outperforms TROPOMI and OMPS in terms of consistency with Pandora ground-based ozone measurements.
- The reprocessed GEMS v2.1 total ozone (O_3T) product still exhibits abnormal geometry-dependent biases.

What are the implications of the main finding?

- The improved O_3P performance highlights the effective implementation of corrections addressing calibration uncertainties.
- The remaining biases in O_3T point to issues in the L1C radiance and irradiance products that need further investigation.

Abstract

This study presents a comprehensive validation of total ozone columns from ozone profile (O_3P) and total ozone column (O_3T) products measured by the Geostationary Environment Monitoring Spectrometer (GEMS), through comparisons with Pandora, Ozone Mapping and Profiler Suite (OMPS) and TROPOspheric Monitoring Instrument (TROPOMI). O_3P version 3.0 demonstrates reduced dependence on viewing geometry compared to version 2.0, whereas the O_3T product shows a consistent offset between versions (v2.0 vs. v2.1). In comparison with Pandora, O_3P exhibits seasonal bias patterns similar to those seen in TROPOMI and OMPS, ranging from −2% in summer to +5% in winter. However, O_3T maintains abnormally persistent negative biases across seasons and times of day, along with a long-term degradation of 2–3% from 2021 to 2024. These findings suggest that O_3T biases likely result from uncorrected radiometric biases rather than algorithmic limitations. Validation metrics further highlight inconsistencies in O_3T, including a lower regression slope (~0.95) in the mid-latitude and higher root mean square errors in the low-latitude (~5%), compared to the other products (near 1.0 and 1–3%, respectively). Overall, O_3P

check for updates

Academic Editor: Manuel Antón

Received: 7 August 2025
Revised: 7 September 2025
Accepted: 18 September 2025
Published: 20 September 2025

Citation: Hong, S.; Bak, J.; Keppens, A.; Yang, K.; Baek, K.; Liu, X.; Kim, M.; Kim, J.; Chang, L.-S.; Lee, H.; et al. Cross-Validation of GEMS Total Ozone from Ozone Profile and Total Column Products Using Pandora and Satellite Observations. *Remote Sens.* **2025**, *17*, 3249. https://doi.org/10.3390/rs17183249

outperforms TROPOMI and OMPS across most validation metrics in mid-latitudes and performs similarly at low latitudes.

Keywords: GEMS; integrated ozone profile; total ozone; validation

1. Introduction

Ozone plays a vital role in Earth's atmosphere by absorbing harmful ultraviolet (UV) radiation in the stratosphere and by influencing air quality and climate in the troposphere [1–3]. Monitoring ozone trends is essential for tracking the recovery of the ozone layer recovery, assessing the effects of ozone-depleting substance (ODS) emissions, and evaluating their contributions to Earth's radiative balance [4–6]. Among various ozone measurement techniques, satellite-based total ozone column (TOC) observations have been widely used owing to their global coverage and long-term records [7–9]. The retrieval of TOC has a long history of algorithm development and validation, achieving accuracies within a few percent [10–12]. However, to detect long-term ozone variations driven by climate change, chlorofluorocarbon (CFC) emissions, and volcanic eruptions, further improvements in the reliability of TOC measurements are still required [13,14]. Even minor uncertainties in satellite observations can propagate into substantial biases in trend analyses; thus, highly accurate and stable TOC measurements are critical for precise ozone monitoring.

The Geostationary Environment Monitoring Spectrometer (GEMS) is the first geostationary satellite dedicated to air quality monitoring over East Asia, providing continuous, high-temporal-resolution observations of ozone and other atmospheric pollutants [15]. This capability is particularly valuable for studying diurnal variations in ozone and regional transport processes. However, the accuracy of GEMS ozone retrievals must be rigorously assessed, as uncertainties in Level 0–1 radiometric calibration and correction procedure can propagate into Level 2 retrievals, potentially affecting their reliability.

GEMS provides two independent ozone datasets: the total ozone column (O_3T), retrieved using a TOMS-based lookup table algorithm [16], and the ozone profile (O_3P), retrieved using an optimal estimation algorithm [17]. Both GEMS O_3T and O_3P were recently reprocessed as versions 2.1 and 3.0, respectively. The O_3T product include only minor updates to the lookup table, whereas the O_3P product incorporates substantial improvements through enhanced wavelength and radiometric calibration [17]. In this study, the O_3P dataset is vertically integrated into total ozone columns to assess its consistency with the O_3T product. This consistency check is essential for verifying the internal reliability of GEMS observations and identifying potential discrepancies arising from uncertainties in spectral measurements.

In general, total ozone validation relies on global ground-based spectrometer networks, including the World Ozone and Ultraviolet Radiation Data Centre (WOUDC), which archives measurements primarily from Dobson and Brewer instruments, and the Pandonia Global Network (PGN), which operates Pandora spectrometers [10,18–20]. Within the GEMS domain, however, only 11 of the 31 WOUDC- registered sites remained operational during 2021–2024 (Figure 1a). Among these, only the Sapporo site provided hourly measurements. On the other hand, the Pandora network has expanded rapidly in recent years, particularly with the establishment of the Pandora Asia Network, to support the validation of GEMS ozone and nitrogen dioxide (NO_2) products [21]. The number of Pandora sites within the GEMS domain increased from 13 in 2021 to 38 in 2024, including 11 located in South Korea (Figure 2b). Accordingly, Pandora measurements are used in this paper as the

primary reference dataset for deriving statistically robust metrics for to evaluate GEMS ozone products.

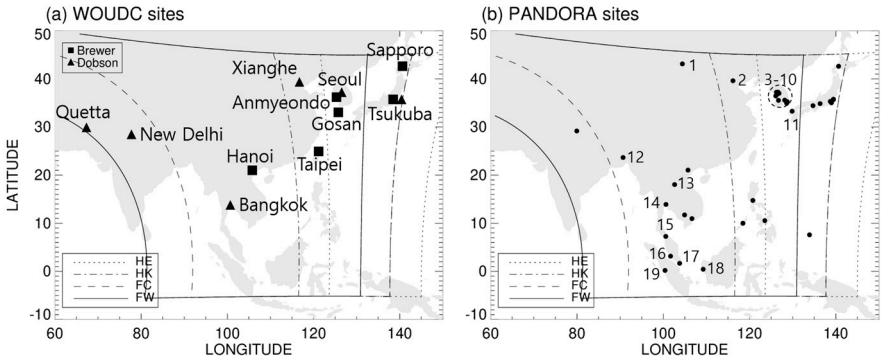

Figure 1. (**a**) Brewer and Dobson sites from the World Ozone and Ultraviolet Radiation Data Centre (WOUDC) network, and (**b**) Pandora sites from the Pandonia Global Network (PGN). The GEMS domain boundaries are indicated with different line styles representing Half East (HE), Half Korea (HK), Full Central (FC), and Full West (FW). For WOUDC, only sites with nearly two years of observations during 2021–2024 were included to exclude discontinued stations. Within the GEMS domains (HE, HK, FC, FW), 39 Pandora sites were operational during 2021–2024. Among these, the Pandora sites in the Full scan domain (FW-FC overlap) with >100 observation days are numbered (1–19) from north to south; sites 3–10 in South Korea are marked with a dashed circle.

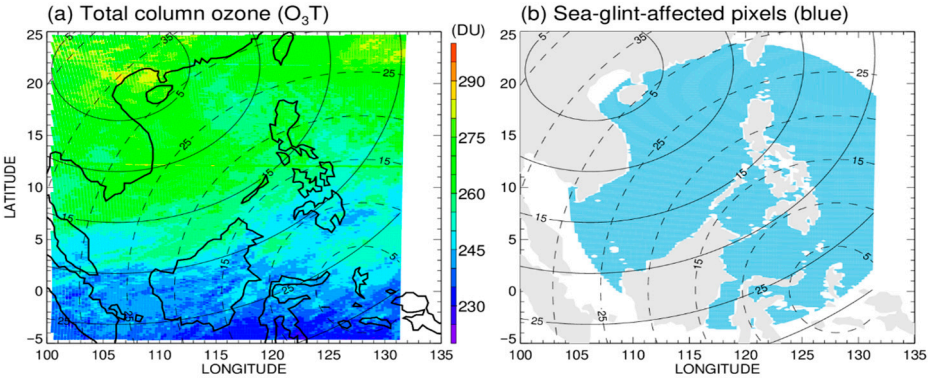

Figure 2. (**a**) GEMS total ozone (O_3T) on 15 July 2023 at 04:45 UTC, and (**b**) corresponding sea-glint–affected pixels (blue). Solid and dashed contours indicate solar zenith angles (SZA) and viewing zenith angles (VZA), respectively, both plotted at 5° intervals.

In addition to ground-based comparisons, satellite-based total ozone products are used to assess the relative performance of GEMS. Similar to the Ozone Monitoring Instrument (OMI) [7], Ozone Mapping and Profiler Suite (OMPS) [22], and TROPOspheric Monitoring Instrument (TROPOMI) [23], GEMS employs a two-dimensional charge-coupled device (CCD) detector. This common instrumental design facilitates cross-satellite validation and supports the harmonization of long-term ozone records. In this study, OMPS and TROPOMI are selected for satellite-based comparisons, while OMI is excluded due to the row anomaly, which resulted in the loss of approximately half of its data [24]. The selected satellite products are utilized to assess the impact of key observational parameters on GEMS products, including solar zenith angle (SZA), viewing zenith angle (VZA), and CCD spatial pixel location, which induces spatially and temporally dependent retrieval errors.

This paper begins by describing the datasets used for cross-validation between satellite products and Pandora, including the collocation criteria and statistical methods (Section 2). The first part of the Results (Section 3.1) presents a comparison between Pandora and two satellite reference products, TROPOMI and OMPS, to identify reliable reference sites and

retrieval characteristics. Sections 3.2 and 3.3 examine the dependence of GEMS ozone retrievals on observational parameters and temporal variations, respectively. Section 3.4 summarizes key validation metrics of the GEMS ozone products. Finally, Section 4 presents the main findings and discussion.

2. Materials and Methods

2.1. Satellite Ozone Products

Table 1 summarizes the key characteristics of GEMS ozone products and total ozone products from the polar-orbiting satellites OMPS/Suomi-NPP and TROPOMI/Sentinel-5P (S5P), used for cross-validation. The GEMS O_3P products have recently been reprocessed to version 3.0, which implements wavelength and radiometric calibrations optimized for the 310–330 nm ozone fitting window [17]. This update significantly reduces the systematic biases identified in the previous version (up to + 40 DU in the troposphere and −20 DU in the stratosphere), resulting in agreement within ± 10 DU when compared with ozonesonde data. In parallel, the GEMS O_3T product has been updated from version 2.0 to version 2.1 following a minor correction in the lookup table implementation. In this study, the impact of the version updates on O_3P and O_3T is evaluated in Section 3.2, with particular emphasis on the retrieval performance's dependency on observational geometry—a known issue in the version 2 product stemming from radiometric calibration uncertainties.

Table 1. Satellite ozone products used for cross-validation, including key instrumental, observational, and algorithmic characteristics.

Satellite Products	**GEMS (O_3P)**	**GEMS (O_3T)**	**OMPS**	**TROPOMI**
Platform	GK-2B		Suomi-NPP	Sentinel-5p
Launch Date	18 February 2020		28 October 2011	13 October 2017
Spatial Resolution (km^2)	14 × 30.8 (4 × 4 binned)	3.5 × 7.7 (no binned) 7.0 × 15.4 (2 × 2 binned) 14 × 30.8 (4 × 4 binned)	50 × 50	3.5 × 5.5 (since August 2019)
Number of spatial (cross-track) pixels	512	512, 1024, 2048 (4 × 4, 2 × 2, 1 × 1)	36	450
Temporal Coverage	07:45–16:45 LT in Korea (geostationary, hourly)		13:30 LT when crossing equator (sun-synchronous)	
Retrieval algorithm (reference)	Optimal Estimation (Bak et al. [17], under review)	TOMS look-up table (Baek et al. [16])	TOMS look-up table (Bhartia et al. [25])	DOAS (Spurr et al. [26])
Ozone cross-section	Birk and Wagner [27]	BDM #	BDM #	Serdyuchenko et al., (2014) [28]

Brion–Daumont–Malicet (Brion et al. [29]; Daumont et al. [30]; Malicet et al. [31])

2.2. Pandora Observations

Pandora is a ground-based UV–visible spectrometer designed to measure direct solar and sky-scattered radiation for the retrieval of total columns of ozone and other trace gases (NO_2, HCHO, and SO_2) [19]. The standard single-spectrometer system (Pandora-1S) covers 280–525 nm with a spectral resolution of 0.6 nm, while the dual-spectrometer system (Pandora-2S) adds a second channel spanning 400–900 nm with 1.1 nm resolution, thereby enabling aerosol characterization [32]. Pandora-1S and Pandora-2S instruments share most of their major components (e.g., fore optics, Sun-and-sky tracker, and data acquisition

system) (https://pandora.gsfc.nasa.gov/Research/RNA/, accessed on 18 September 2025). The instrument operates with a temporal resolution of seconds to minutes throughout the day and achieves clear-sky precision of 0.2% or better. Its standard retrieval algorithm is based on a direct-sun spectral fitting technique similar to Differential Optical Absorption Spectroscopy (DOAS), in which ozone slant column densities are fitted over the 310–330 nm spectral window using absorption cross-sections from the Brion–Daumont–Malicet (BDM) dataset [29–31]. According to Herman et al. [33], applying a geometric air mass factor provides a robust and straightforward approach for converting slant column densities into vertical column densities in direct-sun observations.

The Pandora instruments are globally deployed as part of the PGN, a joint initiative sponsored by the National Aeronautics and Space Administration (NASA) and European Space Agency (ESA). This network includes the Pandora Asia Network (PAN-ASIA) [21], which covers the Korean Peninsula and Southeast Asia. Figure 1b shows the geographic distribution of Pandora sites available for GEMS validation. Of these, 19 sites located within the GEMS full scan domain are included in this study. Most site employ the standard Pandora-1S system, with the exception of the recently established Korean sites since 2023 (Seoul-KU, Yongin). Detailed information about these sites is provided in Table 2.

Table 2. Pandora sites used in this study. Each site is assigned a number corresponding to the labels in Figure 1b. For each site, coordinates (country, longitude, latitude, altitude) and the number of observation days for each year from 2021 to 2024 are provided.

No.	Site Name	Country	Latitude, Longitude (deg)	Altitude (m)	Number of Observation Days			
					2021	2022	2023	2024
1	Dalanzadgad	Mongolia	43.58, 104.42	1466	0	245	365	245
2	Beijing	China	40.00, 116.38	59	166	294	271	0
3 [+]	Seoul-KU	South Korea	37.59, 127.03	90	0	0	0	275
4	Incheon	South Korea	37.57, 126.64	6	158	298	254	366
5	Seoul	South Korea	37.56, 126.93	86	241	271	167	250
6	Seoul-SNU	South Korea	37.46, 126.95	116	339	357	342	341
7 [+]	Yongin	South Korea	37.34, 127.27	122	0	0	214	366
8	Seosan	South Korea	36.78, 126.49	25	230	354	333	330
9	Ulsan	South Korea	35.57, 129.19	38	158	339	298	258
10	Busan	South Korea	35.23, 129.08	71	283	356	286	341
11	Fukuoka	Japan	33.55, 130.37	55	61	364	184	362
12	Dhaka	Bangladesh	23.73, 90.40	34	0	31	365	303
13	Vientiane	Laos	18.00, 102.58	169	0	0	31	366
14	Bangkok	Thailand	13.78, 100.54	60	243	365	365	366
15	Songkhla	Thailand	7.01, 100.50	40	0	153	243	92
16	Banting	Malaysia	2.82, 101.62	7	0	0	276	274
17	Singapore	Singapore	1.30, 103.77	77	0	0	214	366
18	Pontianak	Indonesia	0.04, 109.34	1	0	0	0	306
19	Agam	Indonesia	−0.20, 100.32	865	0	122	334	149

[+] Sites equipped with dual-spectrometer Pandora (2S) systems

2.3. Comparison Methodology

For a fair comparison, we used the total ozone columns derived from the GEMS O_3P product (via integration of ozone profiles) and the GEMS O_3T product. Both products were retrieved at a spatial resolution of 14 × 30.8 km^2 from 4 × 4 binned spectral measurements.

The GEMS O_3P product provides a binary quality flag, indicating either good (0) or bad (1) pixels. Only pixels flagged as good, which are defined as retrievals that have successfully converged with all profile values being positive, were used in this study. The GEMS O_3T product provides a three-level quality flag (good, suspect, bad), where suspect pixels may be affected by factors such as sea-glint, SZA > 84°, or missing cloud fraction. To ensure sufficient data coverage, particularly over low-latitude regions of the western Pacific, both good and sea-glint–affected pixels were included. Figure 2 supports this decision, showing that the impact of sea-glint–affected pixels on total ozone retrievals is negligible. For OMPS, only pixels flagged as good (among the binary classification of good and bad) were used. For TROPOMI, observations with quality flag value less than 0.5 were excluded, following the recommendation of Romahn et al. [34]. For all satellite products, pixels with a cloud-fraction greater than 0.4 were excluded. For Pandora, only observations flagged as high or medium quality were used.

Pandora measurements were collected from 19 sites located within the GEMS Full scan domain, as shown in Figure 1b and Table 2. These measurements are temporally averaged within ±0.5 h of the satellite overpass time and spatially matched to the nearest satellite pixels within a 100 km radius, corresponding to approximately twice the spatial resolution of OMPS. The average distances between Pandora sites and the centers of collocated satellite pixels are 5.5 ± 11.92 km for TROPOMI, 13.77 ± 8.80 km for GEMS, and 30.30 ± 19.23 km for OMPS.

2.4. Validation Metrics

The validation metrics used in this study include the mean bias (MB), 1σ standard deviation (SD), linear regression parameters (slope and offset), correlation coefficient (R), and root mean square error (RMS). To improve statistical robustness, outliers beyond ±3σ from the mean difference were excluded. This threshold helps remove extreme cases and reduce potential sampling imbalance across the GEMS, OMPS, and TROPOMI comparisons with Pandora.

The MB and SD represent the average offset (accuracy) and variability (precision), respectively, of the differences between satellite and reference measurements. These metrics are defined as follows:

$$\boldsymbol{MB} = \frac{1}{\boldsymbol{N}}\sum_{\boldsymbol{i=1}}^{\boldsymbol{N}}(\boldsymbol{S_i} - \boldsymbol{P_i}) \quad (1)$$

$$\boldsymbol{SD} = \sqrt{\frac{\mathbf{1}}{\boldsymbol{N}}\sum_{\boldsymbol{i=1}}^{\boldsymbol{N}}((\boldsymbol{S_i} - \boldsymbol{P_i}) - \boldsymbol{MB})^{\mathbf{2}}} \quad (2)$$

where $\boldsymbol{S_i}$ and $\boldsymbol{P_i}$ denote the satellite and Pandora measurements, respectively, and N is the number of collocated data pairs. The linear regression is expressed as follows:

$$\mathrm{Y} = \mathbf{slope} \times \mathrm{X} + \mathbf{offset} \quad (3)$$

where **Y** represents the satellite retrieval and **X** denotes the Pandora measurements. In addition, the **R** and **RMS** are used to quantify the strength of the linear relationship and the overall magnitude of deviations, respectively.

3. Results

3.1. Intercomparison of Reference Datasets

To ensure the robustness of the validation, we first assessed the internal consistency of the data by comparing total ozone measurements from Pandora, OMPS, and TROPOMI. The high quality of both OMPS and TROPOMI has been demonstrated through extensive validation efforts [12,20]. The latest TROPOMI total ozone Quarterly Operational Validation Report (ROCVR), available at https://mpc-vdaf-server.tropomi.eu/o3-total-column, reports

an overall positive bias of approximately 1.2% with respect to Pandora observations. Notably, Garane et al. [12] reported a high level of consistency (~1%) between OMPS and TROPOMI total ozone retrievals, despite differences in retrieval algorithms and spatial resolutions. These findings align with our validation results shown in Figure 3, which presents the site-by-site MBs and SDs of the relative differences (satellite-pandora) for each year from 2021 to 2024. Overall, both OMPS and TROPOMI are in good agreement with Pandora, showing similar patterns in MB and SD across the stations and years. Notably, the MBs vary from negative values at lower latitudes to positive at higher latitudes, likely reflecting the SZA dependence of satellite observations. In addition, a consistent offset of 1–2% between OMPS and TROPOMI is evident across sites, reflecting differences in either their retrieval algorithms or instrument characteristics. An key factors is the use of different ozone absorption cross-section datasets: OMPS employs the BDM cross-sections, which are consistent with those used in Pandora retrievals and GEMS O_3T, whereas TROPOMI uses an alternative dataset from Serdyuchenko et al. [28]. Furthermore, the SD of relative differences increase toward higher latitudes from 1% to 3%, likely due to enhanced ozone variability at higher latitudes, which amplifies the impact of spatial and temporal mismatches between satellite and ground-based measurements. Accordingly, TROPOMI tends to show slightly smaller SDs than OMPS at most sites, owing to its finer spatial resolution (3.5 × 5.5 km^2 vs. 50 × 50 km^2), which enables more accurate collocation with Pandora measurements.

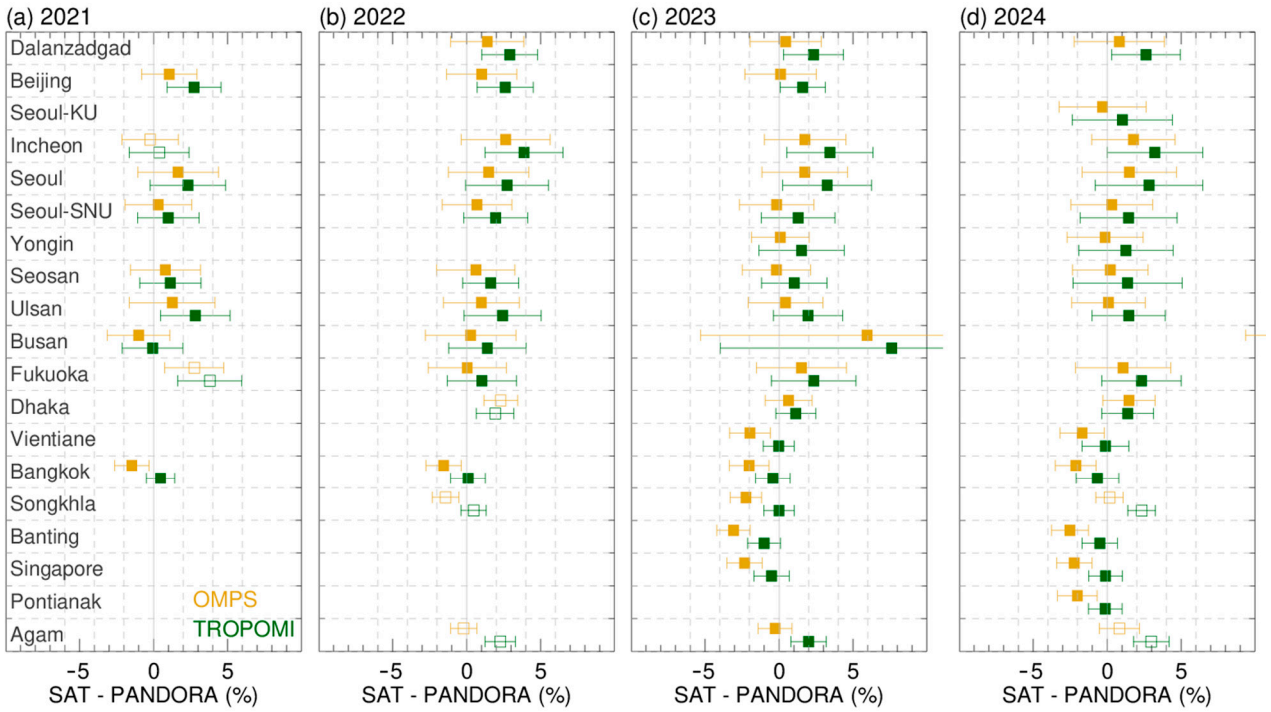

Figure 3. Comparison of OMPS and TROPOMI with Pandora observations from (**a**) 2021, (**b**) 2022, (**c**) 2023, and (**d**) 2024, shown by site from north and south. The mean biases (MBs) of relative differences (%) are plotted using filled (N > 100) and unfilled (N < 100) symbols, with error bars indicating the corresponding 1-σ standard deviation.

The site-by-site comparison reveals the impact of insufficient samplings on mean biases. At Incheon, the 2021 record was concentrated in summer, resulting in smaller biases of 2–3% compared with the full-year sampling in 2022–2024. The 2021 record at Fukuoka was concentrated in winter, leading to higher biases relative to the full-year sampling. Signs of performance degradation in Pandora observations are also detected. At Busan, degradation becomes particularly evident from 2023 onward, as reflected in the markedly elevated MB and SD values. Early signs of degradation were already apparent in 2021

and 2022, when the MB at Busan slightly diverged from those at nearby sites such as Ulsan (~30 km away) and Seosan (~290 km away). This degradation is further supported by Herman et al. [35], who indicated a sun-tracker pointing issue at the Busan site after October 2023. Accordingly, Busan observations are excluded from the subsequent analysis.

To further examine how viewing geometry affects the consistency between satellite and ground-based measurements, the comparison metrics—MB and SD—were calculated by binning the paired total ozone differences in 5° intervals of SZA and VZA (Figure 4). The analysis is limited to 2024, when a greater number of stations were available. Both satellite measurements show increases in MB and SD of about 4–5% and ~1%, respectively, toward higher SZAs, consistent with the latitude-dependent bias patterns noted earlier. In contrast, no clear dependence on VZA is found in either MB or SD. These results support the use of OMPS and TROPOMI as reference datasets for validating GEMS, provided that observations at large SZAs are treated with caution.

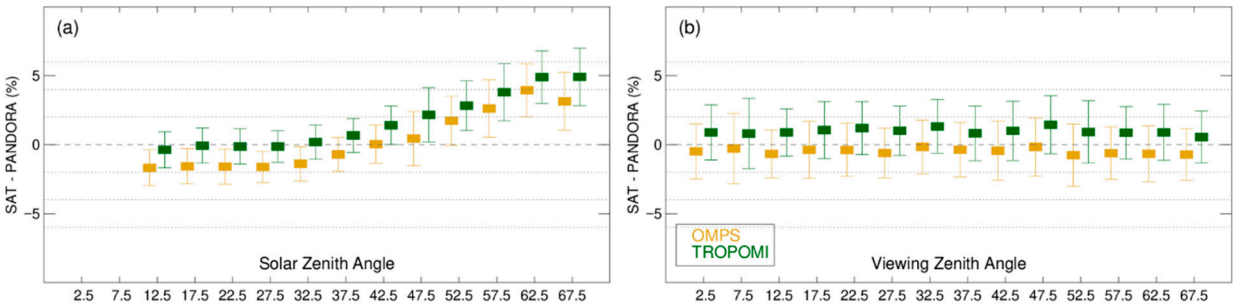

Figure 4. Comparison metrics (mean bias (MB) and standard deviation (SD)) between OMPS/TROPOMI and Pandora for (**a**) solar zenith angle (SZA) and (**b**) viewing zenith angle (VZA), based on one year of data from 2024.

3.2. Dependence of GEMS Ozone Products on Viewing Geometry

The SZA-dependent biases in satellite measurements, as shown in Figure 4a, arise from differences in the atmospheric path length of backscattered photons, which result in reduced sensitivity to the lower atmosphere at high SZAs [36,37]. In addition, VZA-dependent biases are closely associated with cross-track (spatial) pixels, but these biases are negligible for both OMPS and TROPOMI (Figure 4b). Figure 5 compares the SZA-dependent ratios of both GEMS O_3P and O_3T products relative to OMPS, using data collected on the 15th of March, June, September, and December 2021. This comparison also highlights differences between the previous and reprocessed versions of the GEMS ozone products, namely, GEMS O_3P v2.0 vs. v3.0 and GEMS O_3T v2.0 vs. v2.1. The overall SZA dependence remains similar between the two versions of GEMS O_3T, except in December, when the previous version shows a sharp change in the ratios—up to +5% at low SZAs and down to –7% at high SZAs—which is smoothed in the updated version. Nevertheless, the updated version still exhibits a seasonal spread of 7–8%, associated with viewing geometry. However, the GEMS O_3P v3.0 product demonstrates noticeable improvements, including reduced SZA dependence and a narrower seasonal spread (Figure 5a vs. Figure 5b). This suggests that the SZA-dependent features of GEMS O3P v3.0 closely match those of OMPS, leading to cancelation in their ratio—similar to the behavior observed in the comparison between TROPOMI and OMPS (Figure 6a). These improvements are likely attributable to the application of the irradiance offset correction that accounts for Bidirectional Transmittance Distribution Function (BTDF) effects [17]. This correction compensates for radiometric uncertainties in the observed irradiance caused by the observation geometry, and is not applied to the O_3T product. Such BTDF effects are correlated with SZA and VZA-dependent biases and thus contribute to spatial and latitudinal inconsistencies in GEMS measurements

because the spatial pixels of the CCD are aligned from north (high VZA) to south (low VZA). To further assess the impact of viewing geometry, GEMS products are evaluated against OMPS across the GEMS spatial pixels (pixel 1: north to pixel 512: south) on December 15 for each year between 2020 and 2024 (Figure 7). Note that either OMPS or TROPOMI can be used as a reference for this evaluation, since no cross-track dependence is found in comparison of OMPS and TROPOMI (Figure 6b). The previous O_3P version and O_3T v2.0/v2.1 exhibit a distinct gradient in ratios across spatial pixels, with larger spreads in 2022–2024 relative to 2020–2021. The O3P v3.0 product shows improved consistency with OMPS, remaining about −5% across years and spatial pixels. In particular, the O_3T product exhibits a peaked bias for several pixels (e.g., 203th in 2024), indicating imperfect bad pixel flagging in the spectral inputs. This is likely because the O_3T method retrieves ozone by directly matching observations to a precomputed lookup table, without assessing the spectral quality. The O_3P product is derived through spectral fitting and retrieves ozone only when the measured and modeled spectra closely match; thus, it effectively filters out problematic observations. In conclusion, the removal of SZA/VZA dependence in the ratio between GEMS O_3P and OMPS implies that both products share similar satellite measurement characteristics, which likely contribute to the overestimation of total ozone retrievals at higher SZA seen in Figure 4a. The remaining dependence in GEMS O_3T products likely reflects unresolved calibration characteristics.

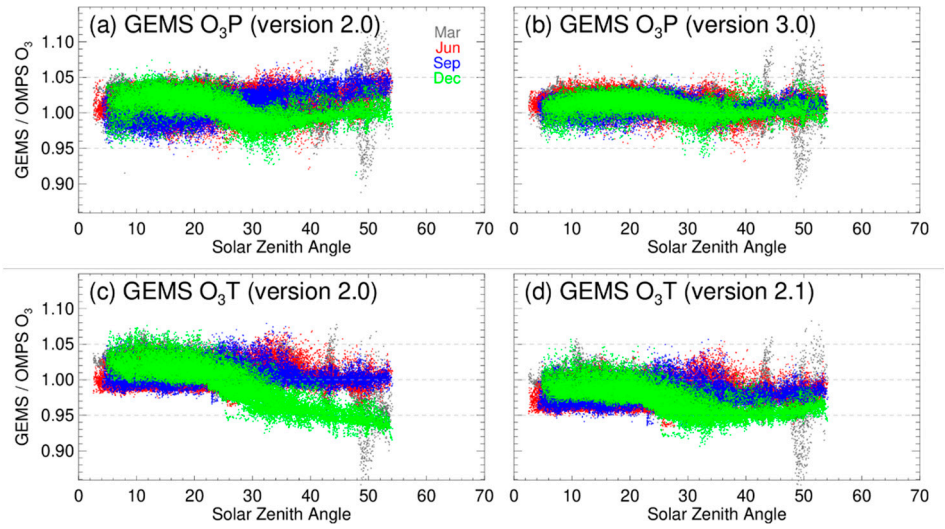

Figure 5. GEMS (04:45 UTC)-to-OMPS total ozone column ratios as a function of SZA for GEMS O_3P ((**a**): version 2.0, (**b**): version 3.0) and O_3T ((**c**): version 2.0, (**d**): version 2.1). Colors represent observations from 15 March, 15 June, 15 September, and 15 December 2021. Among the GEMS reference times, 04:45 UTC is close to the OMPS overpass time over East Asia.

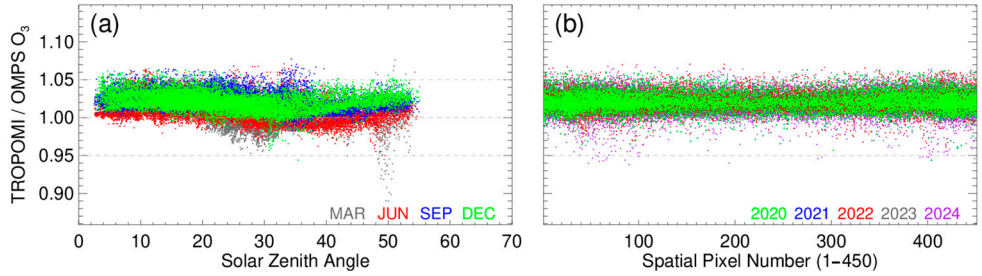

Figure 6. TROPOMI-to-OMPS total ozone column ratios as a function of (**a**) SZA and (**b**) cross-track (spatial pixel) number. To ensure fair sampling, both OMPS and TROPOMI are collocated to GEMS pixels, and the resulting pairs are then used for the TROPOMI–OMPS comparison.

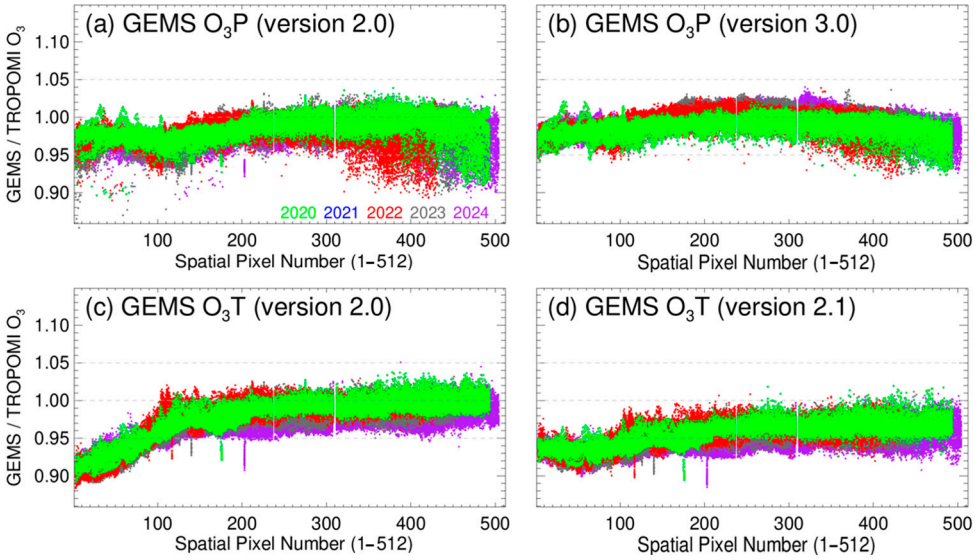

Figure 7. GEMS (04:45 UTC)-to-OMPS total ozone column ratios as a function of GEMS spatial pixel number (1–512). Colors indicate observations from 15 December of each year from 2020 to 2024, all at 04:45 UTC.

3.3. Dependence of GEMS Products on Temporal Variations

This section validates the GEMS ozone products at different temporal resolutions (hourly, monthly, and yearly) through comparisons with Pandora and evaluates their relative accuracy against reference satellite products (OMPS and TROPOMI). The reference dataset is restricted to Pandora sites on the Korean peninsula, which are geographically close to minimize the potential impact of latitudinally dependent biases.

Figure 8 a,b presents the monthly validation results between the satellite products and Pandora in 2021, which was selected to minimize the impact of GEMS instrument degradation. Pandora observations are temporally collocated at 04:45 UTC of GEMS reference time, which corresponds to the overpass time of TROPOMI and OMPS over East Asia. The GEMS O_3P-Pandora comparison exhibits seasonal features similar to those of OMPS and TROPOMI, showing 5–7% discrepancies between summer and winter due to the increasing positive biases during the cold season. These seasonal variations are primarily attributed to common satellite-related characteristics, particularly the influence of atmospheric path length modulated by SZA. On the other hand, the GEMS O_3T product maintains a consistent negative bias of 2–3% relative to Pandora throughout the year. This distinct behavior is likely due to the cancelation effect between the SZA-dependent retrieval errors induced by BTDF and the inherent SZA sensitivity of the satellite measurements. Once BTDF corrections are fully implemented in the Level 0–1 processing, similar seasonal biases may also emerge in the O_3T product. We should note that a radiometric correction to address BTDF effects is implemented in GEMS O_3P v3.0, which likely contributes to its seasonal pattern being consistent with those of OMPS and TROPOMI. The correlation coefficient of the monthly comparisons also shows abnormal no significant differences among the satellite products. However, it tends to be lower during summer (June–August), likely due to reduced atmospheric variability and sampling effects associated with cloud filtering. Figure 8c evaluates the hourly performance of the GEMS products using observations from the warm season (May-September), when seasonal dependence is relatively small. The GEMS O_3T comparison results show no clear variation over the observation times, whereas the O_3P product exhibits increasing discrepancies with Pandora from 04:45 UTC (13:45 LT) to 07:45 UTC (16:45 LT), associated with changes in the SZA (Figure 8d). For long-term assessment, a criterion of at least 200 observations per year is set to ensure

statistical reliability; otherwise, insufficient data sampling could introduce seasonal biases rather than representing the annual mean. Among the stations, four sites met this criterion: Seoul-SNU, Seoul, Seosan, and Bangkok. The results indicate a long-term change in O_3T, with the bias increasing from –2% to –5% (Figure 9). In general, the other products show stable performance with no significant long-term bias.

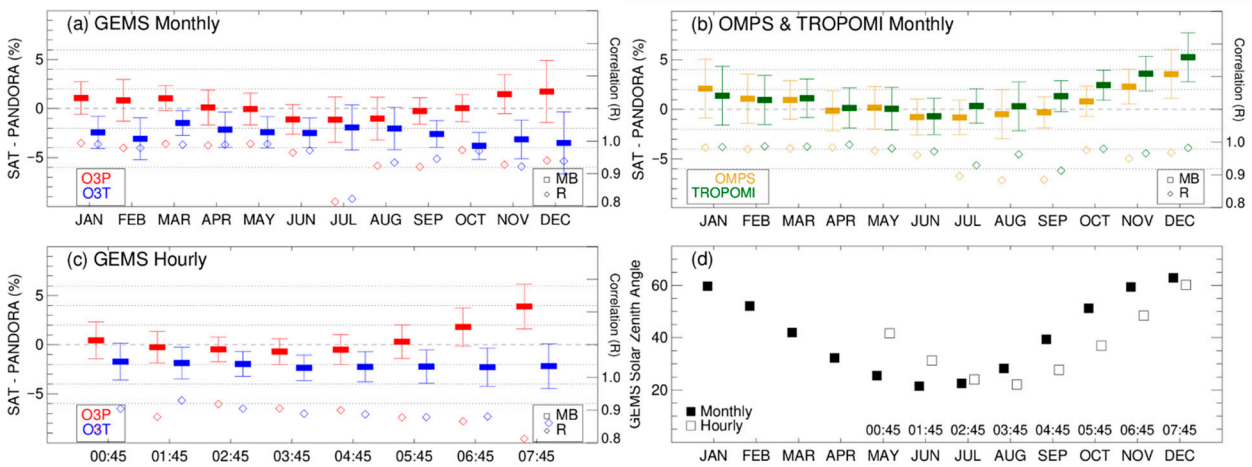

Figure 8. (**a**,**b**) Monthly comparisons of MB and SD (**left** axis) and correlation coefficients (**right** axis) between satellite products and Pandora observations in South Korea at 04:45 UTC in 2021. (**c**) Hourly comparisons between GEMS and Pandora observations during May–September 2021. (**d**) SZAs corresponding to the monthly and hourly data used in panels (**a**) and (**c**), respectively.

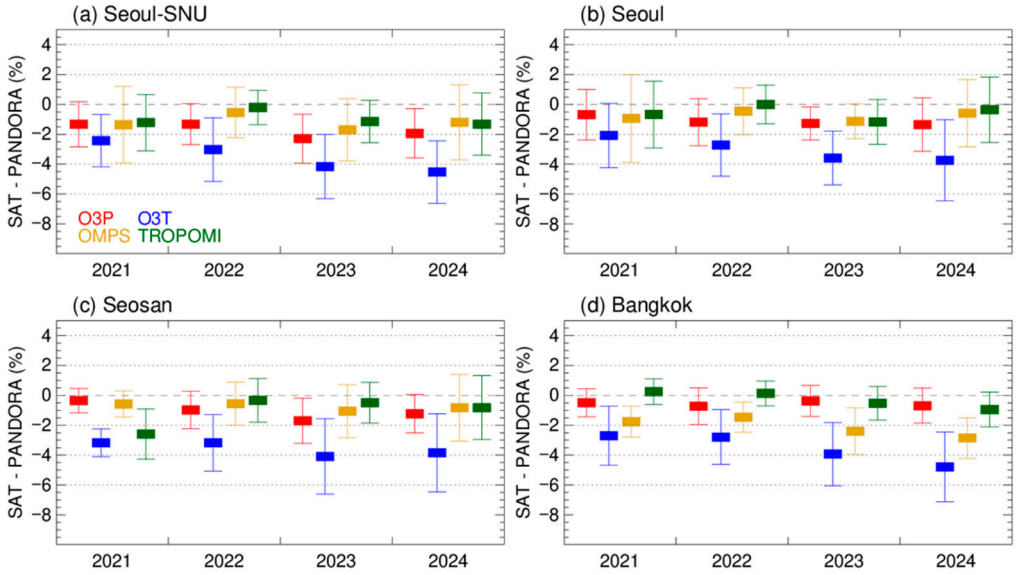

Figure 9. Same as in Figure 8 but for yearly comparison at (**a**) Seoul-SNU, (**b**) Seoul, (**c**) Seosan, and (**d**) Bangkok, respectively.

3.4. Validation Metrics for GEMS Total Ozone Relative to Pandora

To summarize the key validation statistics, the reference dataset is divided into three regional groups: mid-latitude (36.78°N–40.00°N; Beijing, Korean sites), sub-tropical (13.78°N–23.73°N; Dhaka, Vientiane, and Bangkok), and tropical (0.2°S –2.82°N; Banting, Singapore, Pontianak, and Agam). A few stations located in transition zones between regimes are excluded to allow a clear assessment of the latitudinal dependence of performance. The validation metrics described in Section 2.4 are presented in Table 3 for each satellite product across the three regional groups and for each year from 2021 to 2024, except for the sub-

tropical and tropical regions in 2021 and 2022 due to insufficient data. As shown, the O_3P product consistently outperforms the TROPOMI and OMPS over the mid-latitude region across years, achieving a MD of less than 0.5%, SD of 1.7–2.1%, RMS of 1.90–2.28%, and R of 0.98–0.99. However, O_3T exhibits a large MB, both in absolute (−10 DU) and relative terms (−4%). Although the correlation coefficient of O_3T remains stable at 0.99 over the years, its regression slope drops from 0.98 to 0.93, and the RMS increases by 1.7%. For the other products, both the regression slope and RMS remain nearly unchanged, with slopes staying close to 1.0 and RMS increases of less than 0.5%. Overall, the validation results for all satellite products indicate a decline in performance from the mid-latitude to the low-latitude regions, reflected in reduced regression slopes, larger offsets and lower correlation coefficients. This feature is attributable to smaller ozone variability (small total ozone range) and generally lower total ozone amounts [38]. On the other hand, the RMS values tend to improve at lower latitudes, except for O_3T, which exhibits a marked increase from 4.4% in the mid-latitude region to 5–6% in the sub-tropical and tropical regions.

Table 3. Validation statistics of the total ozone column from GEMS O_3P, GEMS O_3T, TROPOMI, and OMPS compared to Pandora measurements. The values are categorized by the region (mid-latitude, sub-tropical, and tropical) and year (2021–2024). Metrics include the number of collocated observations (N), mean bias ± 1σ standard deviation in Dobson Units (DU) and percentage (%), linear regression parameters (slope and intercept), Pearson correlation coefficient (R), and root mean square error (RMS), as defined in Section 2.4.

	Mid-Latitude (36.78°N–40.00°N)			
	2021	**2022**	**2023**	**2024**
O3P	N = 820 2.07 ± 5.49 (DU) 0.60 ± 1.88 (%) y = 1.03x − 8.70 R = 0.99, RMS = 1.88%	N = 1083 1.28 ± 5.77 (DU) 0.40 ± 1.79 (%) y = 1.00x + 2.09 R = 0.99, RMS = 1.97%	N = 977 −0.34 ± 5.75 (DU) −0.12 ± 1.79 (%) y = 1.01x − 3.85 R = 0.98, RMS = 1.93%	N = 1391 −0.55 ± 6.98 (DU) −0.16 ± 2.09 (%) y = 1.00x − 0.61 R = 0.98, RMS = 2.28%
O3T	N = 820 −7.93 ± 4.35 (DU) −2.42 ± 1.31 (%) y = 0.98x − 2.86 R = 0.99, RMS = 2.77%	N = 1083 −10.77 ± 4.73 (DU) −3.25 ± 1.30 (%) y = 0.94x + 9.25 R = 0.99, RMS = 3.50%	N = 977 −13.76 ± 4.95 (DU) −4.21 ± 1.38 (%) y = 0.93x + 9.19 R = 0.99, RMS = 4.44%	N = 1391 −14.62 ± 5.89 (DU) −4.32 ± 1.53 (%) y = 0.92x + 11.26 R = 0.99, RMS = 4.58%
TROPOMI	N = 810 4.72 ± 7.26 (DU) 1.48 ± 2.22 (%) y = 0.98x + 11.17 R = 0.98, RMS = 2.75%	N = 1110 7.90 ± 7.45 (DU) 2.41 ± 2.24 (%) y = 1.02x + 1.92 R = 0.98, RMS = 3.44%	N = 1008 5.71 ± 6.92 (DU) 1.76 ± 2.11 (%) y = 1.02x − 0.32 R = 0.97, RMS = 3.28%	N = 1357 5.50 ± 9.01 (DU) 1.69 ± 2.68 (%) y = 0.99x + 7.56 R = 0.97, RMS = 3.99%
OMPS	N = 816 2.33 ± 7.22 (DU) 0.71 ± 2.22 (%) y = 1.01x − 0.37 R = 0.97, RMS = 2.52%	N = 1121 3.10 ± 7.93 (DU) 0.98 ± 2.43 (%) y = 0.99x + 7.72 R = 0.97, RMS = 2.93%	N = 1004 1.21 ± 8.01 (DU) 0.37 ± 2.46 (%) y = 1.00x − 0.18 R = 0.96, RMS = 2.67%	N = 1392 1.63 ± 9.00 (DU) 0.52 ± 2.69 (%) y = 0.99x + 5.71 R = 0.98, RMS = 2.97%
	Sub-tropical (13.78°N–23.73°N)		**Tropical (0.2°S –2.82°N)**	
	2023	**2024**	**2023**	**2024**
O3P	N = 738 1.52 ± 3.37 (DU) 0.58 ± 1.26 (%) y = 0.95x 15.80 R = 0.97, RMS = 1.53%	N = 702 1.92 ± 3.84 (DU) 0.74 ± 1.44 (%) y = 0.93x + 20.72 R = 0.97, RMS = 1.69%	N = 638 −1.64 ± 4.57 (DU) −0.60 ± 1.73 (%) y = 0.83x +43.19 R = 0.86, RMS = 1.87%	N = 795 −2.09 ± 3.73 (DU) −0.77 ± 1.42 (%) y = 0.89x + 27.47 R = 0.95, RMS = 1.72%

Table 3. *Cont.*

O3T	N = 738 −9.71 ± 3.06 (DU) −3.62 ± 1.12 (%) y = 0.97x − 1.44 R = 0.97, RMS = 3.83%	N = 702 −11.43 ± 3.16 (DU) −4.25 ± 1.15 (%) y = 0.97x − 2.88 R = 0.98, RMS = 4.43%	N = 638 −10.22 ± 6.34 (DU) −3.84 ± 2.34 (%) y = 0.62x + 88.75 R = 0.72, RMS = 4.50%	N = 795 −13.05 ± 4.94 (DU) −4.93 ± 1.78 (%) y = 0.77x + 47.27 R = 0.92, RMS = 5.23%
TROPOMI	N = 705 1.19 ± 4.31 (DU) 0.47 ± 1.60 (%) y = 0.93x + 21.16 R = 0.95, RMS = 1.73%	N = 701 0.36 ± 4.87 (DU) 0.18 ± 1.83 (%) y = 0.89x + 30.43 R = 0.93, RMS = 2.26%	N = 641 0.83 ± 4.70 (DU) 0.34 ± 1.80 (%) y = 0.79x + 55.27 R = 0.84, RMS = 1.84%	N = 769 −0.27 ± 3.32 (DU) −0.08 ±1.29 (%) y = 0.90x +26.75 R = 0.96, RMS = 1.39%
OMPS	N = 685 −1.86 ± 5.81 (DU) −0.67 ± 2.15 (%) y = 0.94x + 14.47 R = 0.92, RMS = 2.31%	N = 702 −3.15 ± 5.85 (DU) −1.14 ± 2.16 (%) y = 0.89x + 27.59 R = 0.92, RMS = 2.59%	N = 608 −4.61 ± 4.51 (DU) −1.74 ± 1.70 (%) y = 0.84x + 38.36 R = 0.86, RMS = 2.43%	N = 740 −5.54 ± 3.53 (DU) −2.11 ± −1.34 (%) y = 0.91x + 18.99 R = 0.96, RMS = 2.53%

4. Discussion

This study presents a comprehensive validation of the GEMS O_3P and O_3T products through cross-comparison with ground-based Pandora measurements and satellite-based OMPS and TROPOMI observations. The site-by-site comparisons between Pandora and OMPS/TROPOMI revealed degraded performance in Pandora measurements at Busan beginning 2023. Furthermore, OMPS and TROPOMI total ozone retrievals commonly exhibited degraded performance at higher SZA, particularly above 40°, although no significant dependence on VZA was observed.

OMPS data were used to assess version updates in the GEMS ozone products. These updates include the implementation of radiometric correction in the O_3P retrieval algorithm (from v2.0 to v3.0) and modifications to the look-up table in the O_3T product (from v2.0 to v2.1). The update to O_3P results in reduced dependence on SZA and VZA as well as improved seasonal and long-term consistency. However, the changes to the O_3T product primarily affected its overall magnitude, with no significant improvements in retrieval characteristics related to viewing geometry or temporal variation.

We also performed a cross-evaluation of GEMS, OMPS, and TROPOMI ozone products against Pandora measurements to assess the relative performance of these satellite products. A similar seasonal bias pattern was observed in the GEMS O_3P, OMPS, and TROPOMI products, with values ranging from –2% in summer to +5% in winter. Importantly, none of these products exhibited any signs of long-term degradation over the 2021–2024 period. However, the GEMS O_3T revealed a persistent offset against Pandora without seasonal and hourly patterns, along with a degradation trend of approximately 2–3%. Validation metrics further confirmed that the O_3P product outperformed OMPS and TROPOMI in most metrics over the mid-latitude, while performing similarly to the other products in the low-latitude. These findings suggest that the O_3T biases likely arise from uncorrected calibration artifacts, rather than algorithmic limitations. Validation metrics also highlighted inconsistencies in the O_3T product, including a lower regression slope (~0.95) in the mid-latitude compared to the other products (near 1.0) and higher RMS errors in the low-latitude (~5%) compared to O_3P (2–3%) and other satellite datasets.

This validation study not only confirmed the improved performance of the reprocessed O_3P product (v3.0) but also identified key issues in the O_3T product that merit further investigation. The O_3P product demonstrates performance comparable to that of other satellite instruments, highlighting the effective implementation of the applied correction to address calibration uncertainties.

Author Contributions: Conceptualization, J.B. and J.-H.K.; Methodology, J.B., K.Y. and X.L.; Software, J.B. and S.H.; Validation, S.H.; Formal analysis, J.B. and A.K.; Data curation, S.H.; Writing—original draft, J.B.; Writing—review and editing, J.B., S.H., J.-H.K., A.K., K.Y., K.B., X.L., M.K., J.K., L.-S.C. and H.L. All authors have read and agreed to the published version of the manuscript.

Funding: The research reported in this article was supported by the Basic Science Research Program of the National Research Foundation of Korea (NRF), funded by the Ministry of Education (grant numbers RS-2020-NR049592 and RS-2021-NR058144). Additional support was provided by a grant from the National Institute of Environment Research (NIER), funded by the Ministry of Environment (MOE) of the Republic of Korea (grant no. NIER-2025-04-02-063).

Data Availability Statement: GEMS products are available from the Environmental Satellite Center website (https://nesc.nier.go.kr/en/html/datasvc/index.do, accessed on 18 September 2025). OMPS and TROPOMI products can be downloaded from NASA's GES DISC (https://disc.gsfc.nasa.gov/datasets/, accessed on 18 September 2025) and the Copernicus Data Space Ecosystem (CDSE, https://dataspace.copernicus.eu/, accessed on 18 September 2025), respectively. Pandora total ozone measurements from the Pandonia Global Network (PGN) are available at https://data.hetzner.pandonia-global-network.org/, accessed on 18 September 2025.

Acknowledgments: We gratefully acknowledge the GEMS science team and the Environmental Satellite Center (ESC) of the National Institute of Environmental Research (NIER) for their support in developing the GEMS ozone profile and total column retrieval algorithms. We also thank the TEMPO, PEGASUS, OMPS, TROPOMI (S5P), and Pandora teams for their valuable contributions to algorithm development and product validation.

Conflicts of Interest: The authors declare no conflicts of interest.

References

1. Isaksen, I.S.A.; Granier, C.; Myhre, G.; Berntsen, T.K.; Dalsøren, S.B.; Gauss, M.; Klimont, Z.; Benestad, R.; Bousquet, P.; Collins, W.; et al. Atmospheric composition change: Climate–Chemistry interactions. *Atmos. Environ.* **2009**, *43*, 5138–5192. [CrossRef]
2. Monks, P.S.; Archibald, A.T.; Colette, A.; Cooper, O.; Coyle, M.; Derwent, R.; Fowler, D.; Granier, C.; Law, K.S.; Mills, G.E.; et al. Tropospheric ozone and its precursors from the urban to the global scale from air quality to short-lived climate forcer. *Atmos. Chem. Phys.* **2015**, *15*, 8889–8973. [CrossRef]
3. Solomon, S. Stratospheric ozone depletion: A review of concepts and history. *Rev. Geophys.* **1999**, *37*, 275–316. [CrossRef]
4. Chipperfield, M.P.; Bekki, S.; Dhomse, S.; Harris, N.R.P.; Hassler, B.; Hossaini, R.; Steinbrecht, W.; Thiéblemont, R.; Weber, M. Detecting recovery of the stratospheric ozone layer. *Nature* **2017**, *549*, 211–218. [CrossRef]
5. Chipperfield, M.P.; Bekki, S. Opinion: Stratospheric ozone—Depletion, recovery and new challenges. *Atmos. Chem. Phys.* **2024**, *24*, 2783–2802. [CrossRef]
6. Weatherhead, E.C.; Andersen, S.B. The search for signs of recovery of the ozone layer. *Nature* **2006**, *441*, 39–45. [CrossRef]
7. Levelt, P.F.; Joiner, J.; Tamminen, J.; Veefkind, J.P.; Bhartia, P.K.; Stein Zweers, D.C.; Duncan, B.N.; Streets, D.G.; Eskes, H.; van der A, R.; et al. The Ozone Monitoring Instrument: Overview of 14 years in space. *Atmos. Chem. Phys.* **2018**, *18*, 5699–5745. [CrossRef]
8. McPeters, R.D.; Frith, S.; Labow, G.J. OMI total column ozone: Extending the long-term data record. *Atmos. Meas. Tech.* **2015**, *8*, 4845–4850. [CrossRef]
9. Weber, M.; Arosio, C.; Coldewey-Egbers, M.; Fioletov, V.E.; Frith, S.M.; Wild, J.D.; Tourpali, K.; Burrows, J.P.; Loyola, D. Global total ozone recovery trends attributed to ozone-depleting substance (ODS) changes derived from five merged ozone datasets. *Atmos. Chem. Phys.* **2022**, *22*, 6843–6859. [CrossRef]
10. Bak, J.; Liu, X.; Kim, J.H.; Chance, K.; Haffner, D.P. Validation of OMI total ozone retrievals from the SAO ozone profile algorithm and three operational algorithms with Brewer measurements. *Atmos. Chem. Phys.* **2015**, *15*, 667–683. [CrossRef]
11. Balis, D.; Kroon, M.; Koukouli, M.E.; Brinksma, E.J.; Labow, G.; Veefkind, J.P.; McPeters, R.D. Validation of Ozone Monitoring Instrument total ozone column measurements using Brewer and Dobson spectrophotometer ground-based observations. *J. Geophys. Res. Atmos.* **2007**, *112*, D07307. [CrossRef]
12. Garane, K.; Koukouli, M.-E.; Verhoelst, T.; Lerot, C.; Heue, K.-P.; Fioletov, V.; Balis, D.; Bais, A.; Bazureau, A.; Dehn, A.; et al. TROPOMI/S5P total ozone column data: Global ground-based validation and consistency with other satellite missions. *Atmos. Meas. Tech.* **2019**, *12*, 5263–5287. [CrossRef]
13. Chehade, W.; Weber, M.; Burrows, J.P. Total ozone trends and variability during 1979–2012 from merged data sets of various satellites. *Atmos. Chem. Phys.* **2014**, *14*, 7059–7074. [CrossRef]

14. Fleming, E.L.; Newman, P.A.; Liang, Q.; Daniel, J.S. The Impact of Continuing CFC-11 Emissions on Stratospheric Ozone. *J. Geophys. Res. Atmos.* **2020**, *125*, e2019JD031849. [CrossRef]
15. Kim, J.; Jeong, U.; Ahn, M.-H.; Kim, J.H.; Park, R.J.; Lee, H.; Song, C.H.; Choi, Y.-S.; Lee, K.-H.; Yoo, J.-M.; et al. New era of air quality monitoring from space: Geostationary environment monitoring spectrometer (GEMS). *Bull. Am. Meteorol. Soc.* **2020**, *101*, E1–E22. [CrossRef]
16. Baek, K.; Kim, J.H.; Bak, J.; Haffner, D.P.; Kang, M.; Hong, H. Evaluation of total ozone measurements from Geostationary Environmental Monitoring Spectrometer (GEMS). *Atmos. Meas. Tech.* **2023**, *16*, 5461–5478. [CrossRef]
17. Bak, J.; Keppens, A.; Choi, D.; Hong, S.; Kim, J.-H.; Kim, C.-H.; Lee, H.-J.; Jeon, W.; Kim, J.; Koo, J.-H.; et al. GEMS ozone profile retrieval: Impact and validation of version 3.0 improvements. *EGUsphere* **2025**. *under review*. [CrossRef]
18. Baek, K.; Bak, J.; Kim, J.H.; Park, S.S.; Haffner, D.P.; Lee, W. Validation of geostationary environment monitoring spectrometer (GEMS), TROPOspheric Monitoring Instrument (TROPOMI), and Ozone Mapping and Profiler Suite Nadir Mapper (OMPS) using pandora measurements during GEMS Map of Air Pollution (GMAP) field campaign. *Atmos. Environ.* **2024**, *324*, 120408. [CrossRef]
19. Herman, J.; Evans, R.; Cede, A.; Abuhassan, N.; Petropavlovskikh, I.; McConville, G. Comparison of ozone retrievals from the Pandora spectrometer system and Dobson spectrophotometer in Boulder, Colorado. *Atmos. Meas. Tech.* **2015**, *8*, 3407–3418. [CrossRef]
20. Herman, J.; Evans, R.; Cede, A.; Abuhassan, N.; Petropavlovskikh, I.; McConville, G.; Miyagawa, K.; Noirot, B. Ozone comparison between Pandora #34, Dobson #061, OMI, and OMPS in Boulder, Colorado, for the period December 2013–December 2016. *Atmos. Meas. Tech.* **2017**, *10*, 3539–3545. [CrossRef]
21. Chang, L.-S.; Kim, D.; Hong, H.; Kim, D.-R.; Yu, J.-A.; Lee, K.; Lee, H.; Kim, D.; Hong, J.; Jo, H.-Y.; et al. Evaluation of correlated Pandora column NO_2 and in situ surface NO_2 measurements during GMAP campaign. *Atmos. Chem. Phys.* **2022**, *22*, 10703–10720. [CrossRef]
22. Flynn, L.; Long, C.; Wu, X.; Evans, R.; Beck, C.T.; Petropavlovskikh, I.; McConville, G.; Yu, W.; Zhang, Z.; Niu, J.; et al. Performance of the Ozone Mapping and Profiler Suite (OMPS) products. *J. Geophys. Res. Atmos.* **2014**, *119*, 6181–6195. [CrossRef]
23. Veefkind, J.P.; Aben, I.; McMullan, K.; Förster, H.; de Vries, J.; Otter, G.; Claas, J.; Eskes, H.J.; de Haan, J.F.; Kleipool, Q.; et al. TROPOMI on the ESA Sentinel-5 Precursor: A GMES mission for global observations of the atmospheric composition for climate, air quality and ozone layer applications. *Remote Sens. Environ.* **2012**, *120*, 70–83. [CrossRef]
24. Schenkeveld, V.M.E.; Jaross, G.; Marchenko, S.; Haffner, D.; Kleipool, Q.L.; Rozemeijer, N.C.; Pepijn Veefkind, J.; Levelt, P.F. In-flight performance of the Ozone Monitoring Instrument. *Atmos. Meas. Tech.* **2017**, *10*, 1957–1986. [CrossRef]
25. Bhartia, P.K.; Wellemeyer, C. TOMS-V8 Total O3 Algorithm, in OMI Algorithm Theoretical Basis Document, vol. II, OMI Ozone Products, ATBD-OMI-02, Edited by P. K. Bhartia, pp. 15–31, NASA Goddard Space Flight Cent., Greenbelt, Md. 2002. Available online: https://eospso.nasa.gov/sites/default/files/atbd/ATBD-OMI-02.pdf (accessed on 18 September 2025).
26. Spurr, R.; Loyola, D.; Heue, K.-P.; Van Roozendael, M.; Lerot, C. S5P/TROPOMI Total Ozone ATBD. S5P-L2-DLR-ATBD-400A, Issue 2.4. 2022. Available online: https://sentiwiki.copernicus.eu/ (accessed on 18 September 2025).
27. Birk, M.; Wagner, G. ESA SEOM-IAS—Measurement and ACS database O3 UV region (I). *Zenodo* **2018**. [CrossRef]
28. Serdyuchenko, A.; Gorshelev, V.; Weber, M.; Chehade, W.; Burrows, J.P. High spectral resolution ozone absorption cross-sections—Part 2: Temperature dependence. *Atmos. Meas. Tech.* **2014**, *7*, 625–636. [CrossRef]
29. Brion, J.; Chakir, A.; Daumont, D.; Malicet, J.; Parisse, C. High-resolution laboratory absorption cross section of O3. Temperature effect. *Chem. Phys. Lett.* **1993**, *213*, 610–612. [CrossRef]
30. Daumont, D.; Brion, J.; Charbonnier, J.; Malicet, J. Ozone UV spectroscopy I: Absorption cross-sections at room temperature. *J. Atmos. Chem.* **1992**, *15*, 145–155. [CrossRef]
31. Malicet, J.; Daumont, D.; Charbonnier, J.; Parisse, C.; Chakir, A.; Brion, J. Ozone UV spectroscopy. II. Absorption cross-sections and temperature dependence. *J. Atmos. Chem.* **1995**, *21*, 263–273. [CrossRef]
32. Kim, S.; Jeong, U.; Lee, H.; Jung, Y.; Kim, J.H. Assessments of the GEMS NO_2 Products Using Ground-Based Pandora and In-Situ Instruments over Busan, South Korea. *Korean J. Remote Sens.* **2024**, *40*, 1–8. [CrossRef]
33. Herman, J.; Cede, A.; Spinei, E.; Mount, G.; Tzortziou, M.; Abuhassan, N. NO_2 column amounts from ground-based Pandora and MFDOAS spectrometers using the direct-sun DOAS technique: Intercomparisons and application to OMI validation. *J. Geophys. Res. Atmos.* **2009**, *114*, D13307. [CrossRef]
34. Romahn, F.; Pedergnana, M.; Loyola, D.; Apituley, A.; Sneep, M.; Veefkind, J.P. Sentinel-5 Precursor/TROPOMI Level 2 Product User Manual: O3 Total Column. S5P-L2-DLR-PUM-400A, Issue 2.4.0. 2022. Available online: https://sentinels.copernicus.eu/documents/247904/2474726/Sentinel-5P-TROPOMI-Level-2-Product-User-Manual-Ozone-profiles.pdf (accessed on 18 September 2025).
35. Herman, J.; Mao, J.; Huang, L.; Cede, A. Validation of DSCOVR-EPIC Total Column O3 Retrievals Using Ground-Based Pandora as well as OMPS, OMI, and TEMPO Satellite Data. *Front. Remote Sens.* **2025**, *6*, 1623828. [CrossRef]

36. Bak, J.; Kim, J.H.; Spurr, R.J.D.; Liu, X.; Newchurch, M.J. Sensitivity study of ozone retrieval from UV measurements on geostationary platforms. *Remote Sens. Environ.* **2012**, *118*, 309–319. [CrossRef]
37. Klenk, K.F.; Bhartia, P.K.; Kaveeshwar, V.G.; McPeters, R.D.; Smith, P.M.; Fleig, A.J. Total ozone determination from the Backscattered Ultraviolet (BUV) Experiment. *J. Appl. Meteor. Climatol.* **1982**, *21*, 1672–1684. [CrossRef]
38. Huang, X.; Yang, K. Algorithm theoretical basis for ozone and sulfur dioxide retrievals from DSCOVR EPIC. *Atmos. Meas. Tech.* **2022**, *15*, 5877–5915. [CrossRef]